Proceedings of the 2005 IEEE
International Conference on Mechatronics
July 10-12, 2005, Taipei, Taiwan

Design for Control of a Flexure Jointed Optical Servo Scanning Platform

Yea-Chin Yeh [1], Jia-Yush Yen[2] and Yung-Hao Peng [3]
[3]Graduate student, [1]PhD candidate, [2]Professor,
Department of Mechanical Engineering
National Taiwan University
No.1 Sec.4 Roosevelt Rd., Taipei, Taiwan 10617, ROC
F9152281@ntu.edu.tw

Jyh-Fa Lee[4]
[4]Deputy chief technical superintendent, *Materials & Elecrto-Optics Research Division, Electro-Optical Section*
Chung-Shan institute of science & technology
Lung-Tan, Tao-Yuan, Taiwan 32599, ROC
omystart@yahoo.com.tw

Abstract **- High resolution and precision servo mechanism has played an important role in micro and nano optics. Its application includes projection systems, head-mount displays, scanners, cameras, heat tracking systems and so on... The servo mechanisms are often used to enhance the optical resolution by driving the scanning mirrors to reach position resolution far beyond the conventional optical systems. It is often necessary for these servo mechanisms to achieve high operation speeds while maintaining extreme positioning accuracy. To achieve this goal, this paper introduces a novel, high speed, high precision servo mechanism [1] for an optical scanning platform. The proposed design uses piezoelectric transducers (PZT) with flexure joints. The use of the flexure joints not only eliminates backlash to achieve smooth and continuous displacement but also reduces friction to eradicate the need for lubrication. In order to understand the basic dynamics of the platform, this paper uses ANSYS for the finite element analysis (FEA) of all the desirable physical properties of the mechanism. The FEA analysis is also used for simulating the dynamic behavior of the control system. Based on the simulation results an improved controller is constructed for better scanning resolutions.**

Index Terms - optical scanning platform, PZT actuator, FEA

I. INTRODUCTION

Modern optical systems rely on scanning platform not only to enlarge the field of view but also to enhance the viewing resolution. Lately a new step-and-scan design shown in Fig. 1 is getting increased attention, particularly for systems design for long distance and large field operation. As shown in fig. 1, there are 4n steps in the step-scan path. It is evident that more scanning steps resulted in slower scanning speed. The design concerns thus turn to operating in a high frequency with a very fine resolution. This is because the time duration between the consecutive control steps must cover the signal acquisition time and the image processing time. These kinds of image processing systems usually try to first obtain a front view, and then reconstruct the image by an array of area (or linear) CCD (or COMS) detectors. The signal from a single CCD or COMS detector scan can only represent a portion of the front view. The accuracy of the scanning platform is thus essential to the successful reconstruction of a truthful picture. For a smooth operation, the servo system has to incorporate certain amount of time delay during each servo step to allow for the image data acquisition. Thus, the stepping motion requires not only a precision positioning control but also a mechanism that can release a very large torque upon request. On top of that the high torque demand leads to an addition size difficulty. From the conventional servo design point of view, high torque actuator and drive mechanisms always take up large spaces. It is thus desirable to come up with a design that achieves fast movement without taking up too much space. This paper describes a new optical scanning system design. The proposed system uses PZT actuators with flexure joints in place of the conventional servo actuators [2][3]. The PZT actuators are widely used in micro-manipulation because of the convenient properties of small size, high force transmission, rapid response and easy control [4]. To understand the basic dynamic motion of the platform, the study used the FEA software to conduct simulation and to study the possible physical phenomena of the mechanism. The simulation results and the experimental results are compared. The comparisons suggested an improved PID controller that mimics the behaviour of the popular learning control. The experimental results with the proposed algorithm showed better performances with decreased tracking errors and shorter response times.

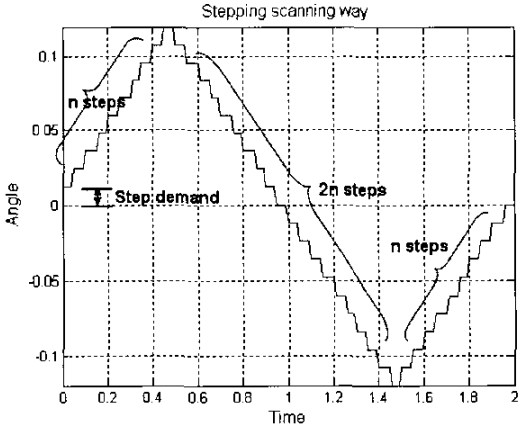

Fig.1 Step-scan way.

II. THE ARCHITECTURE OF THE SYSTEM

The rough design chart of the novel high speed optical scanning platform is shown in Fig. 2. The scanning

method is to control displacements of PZT actuators "A", "B" precisely by adding contrary voltages to PZT actuators so that flexure joints "a" and "b" will move in opposite directions. The platform motion is obtained by LVDT position sensors "C", "D" continuously to complete the feedback control as shown in Fig. 3.

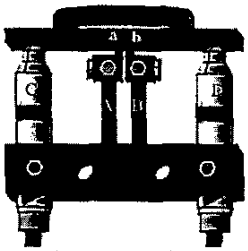

. Fig. 2 Design Chart.

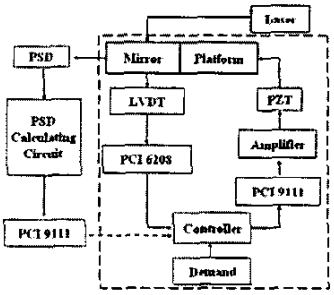

Fig. 3 Control process.

First, switch on the laser and the PSD detecting device and then give the demand. The AD card transmits the control output to the amplifier as the input of PZT actuators. Get the position data from LVDT sensors and then feedback to the controller. The resolution limit of LVDT sensors are down to 10 nm. In order to verify the precision simultaneously, the four phase PSD detecting device also feedback the true position data of the reflected laser points. The linear sensing range of PSD is around 2mm for that reason we put PSD sensor near the scanner. Use DA cards to transform signals into the controller. The marked rectangular area with dotted lines is the initial designed system. The dimensions of the PZT actuator is 2 × 3 × 18 mm^3 and the material properties are provided in Table 1. The stage is made of aluminum and the material properties are provided in Table 2.

Table 1. Material properties of the PZT

N-10		
s^E_{11}	14.8×10^{-12}	m^2/N
s^E_{33}	18.4×10^{-12}	m^2/N
d_{15}	930×10^{-12}	m/V
d_{31}	-287×10^{-12}	m/V
d_{33}	635×10^{-12}	m/V
$\varepsilon^S_{11}/\varepsilon_0$	5000	
$\varepsilon^S_{33}/\varepsilon_0$	5440	
Density	8000	kg/m^3

Table 2. Material properties of aluminum

7079_T2		
Elastic modulus	$7.17e^{10}$	Pa
Yield stress	$3.45e^8$	Pa
Ultimate tensile stress	$4.83e^8$	Pa
Poisson's ratio	0.33	
Thermal conductivities	121	W/mK
Specific heat	963	Nm/kgK
Density	2740	kg/m^3

III. FEA simulation software

FEM simulation was carried out using FEM software (ANSYS 8.0 [5]), which was used to create a solid FE model for modal-frequency and harmonic response analyses. We use modal analysis to determine the natural frequencies and mode shapes of a structure. The natural frequencies and mode shapes are important parameters in the design of a structure for dynamic loading conditions. They are also required if you want to do a spectrum analysis or a mode superposition harmonic or transient analysis. The simulated natural frequencies are illustrated in Table 3. The mode shapes of a structure after modal analysis are shown in Fig. 4 to Fig. 9. The dynamic motion of the 1st mode is the Z direction torsional oscillation of flexure joints. The 2nd mode is the X direction torsional oscillation of flexure joints and the PZT actuators. The 3rd mode is the Y direction torsional oscillation of flexure joints and the PZT actuators. The deformation of this mode is larger than 1st and 2nd mode. The 4th mode is the up and down oscillation of the diagonal apexes and the edges in the different direction at Z direction and the deformation is even larger than previous results. This oscillation way is exactly like our scanning way. The 5th mode is the same as the 2nd mode. The 6th mode is up and down oscillation of the edge in the same direction in Z direction.

Table 3.Modal frequency

Mode number	Frequency (Hz)
1	522.54
2	681.45
3	831.03
4	1184.2
5	2693.1
6	4061.6

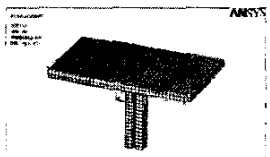

Fig. 4 Mode shape of mode 1.

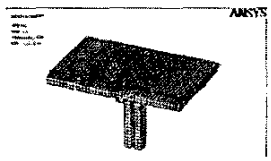

Fig. 5 Mode shape of mode 2.

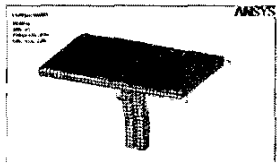

Fig. 6 Mode shape of mode 3.

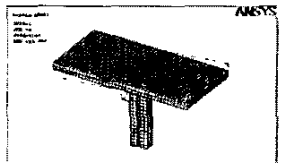

Fig. 7 Mode shape of mode 4.

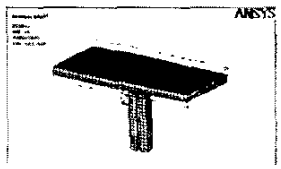

Fig. 8 Mode shape of mode 5.

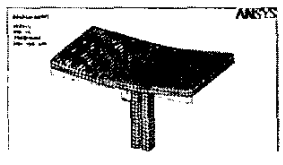

Fig. 9 Mode shape of mode 6.

Harmonic response analysis gives us the ability to predict the sustained dynamic behaviour of structures, thus enabling us to verify whether or not designs will successfully overcome the resonance, fatigue, and other harmful effects of forced vibrations. This analysis technique calculates only the steady-state, forced vibrations of a structure. The transient vibrations, which occur at the beginning of the excitation, are not accounted

for in a harmonic response analysis. The harmonic analysis result is shown in Fig. 10. The frequency range is from 1 Hz to 50K Hz with 500 sub steps, which means that every 100Hz calculate once. There are 5 main natural frequencies which may make the structure fatigue especially the resonance frequency within 20K-25K Hz. In view of the fact the working speed is not so such big. We re-simulate the harmonic analysis which is shown in Fig. 11. The frequency range is from 1Hz to 5K Hz with 100 sub steps.

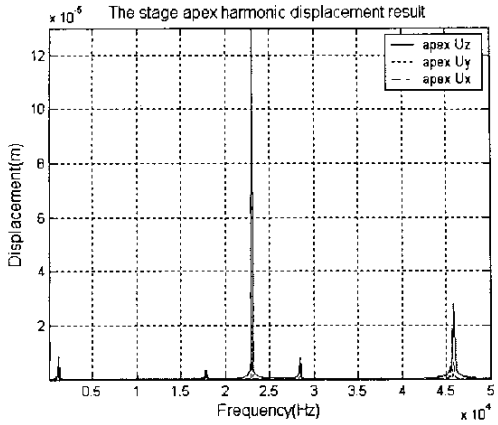

Fig. 10 Harmonic analysis result from 0 to 50k Hz.

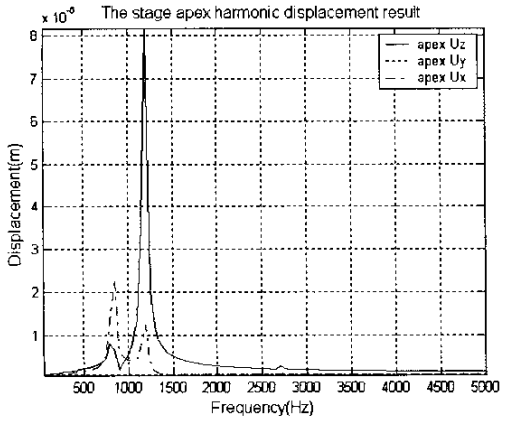

Fig. 11 Harmonic analysis result from 0 to 5k Hz.

The above analysis results express some thing. First, in 3rd mode the deformation in X direction may bigger than in Y direction. We should avoid operating the platform around the 3rd natural frequency. The dynamic motion of the 4th mode is exactly the same as our demanded scanning way. May be we can try to operate our system at this resonance frequency to obtain larger scanning range.

The transient analysis solution method used depends on the DOFs involved. For matrix coupling between first and second order effects such as for piezoelectric analysis, a combined procedure is used. We have to know that whether the physical properties in transient analysis results and the real implement results is the same or not, so as to raise the reliability of the transient analysis results and to prove the accuracy of the parameters. Hence we run a PID control in transient analysis. The close loop control is to get every sub step analysis results and saving it to be the feedback of the next sub step analysis. The transient step reference PID control is shown in Fig. 12. The physical phenomenon is almost the same to the experiment although the FEA simulation result had added a multiple. That is because in real experiment we used multilayer PZT actuators but in analysis we take it as a stack PZT actuator. It proves that the transient results are believable. Consequently we tried to simulate the transient PID control under the step-scan mode reference and analysis results are illustrated in Fig. 13.

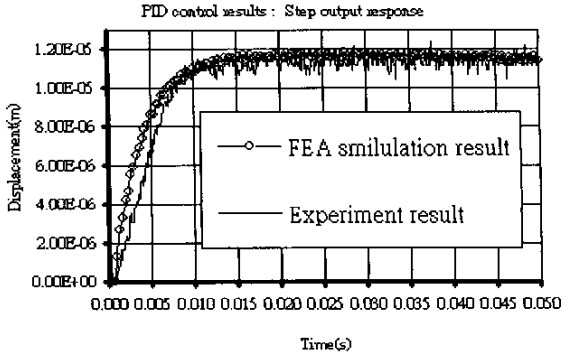

Fig. 12 Transient analysis PID control result with step reference.

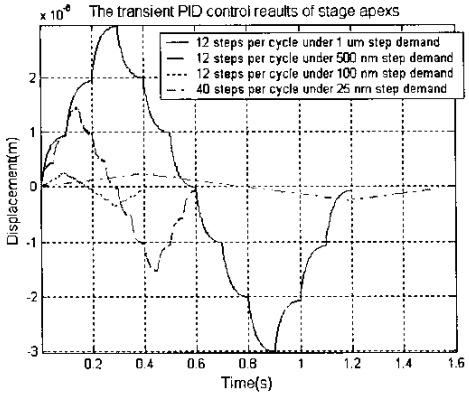

Fig. 13 PID control result with step-scan reference.

IV. EXPERIMENT

Besides to use PID controller shown in Fig. 14 doing the basic control and getting the control results, this paper establishes an improved PID controller to acquire better control performance. The PID control results are illustrated in Fig. 15 and Fig. 16. Fig. 15 is the 1024 resolution steps, 1 Hz repeat scanning result. The control results appears that that the feedback signals from LVDT and the PSD sensors are almost the same. That means the settling response of each step within 1/1024 s is sufficient.

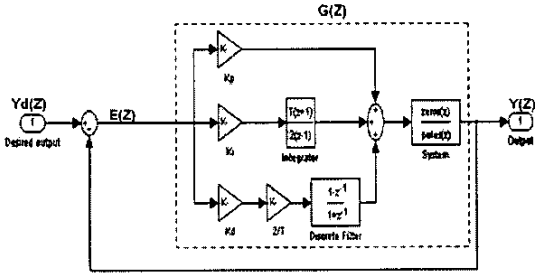

Fig. 14 PID control block diagram.

Fig. 16 is the 128 resolution steps, 30 Hz repeat scanning result. The control results appears that that the feedback signals from LVDT and the PSD sensors are different and not accurate. That means the settling response of each step within 1/(128*30) s is not sufficient.

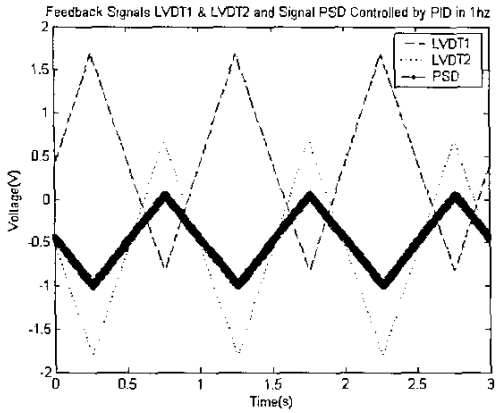

Fig. 15 PID control, 1024 resolution steps, 1 Hz repeat scanning.

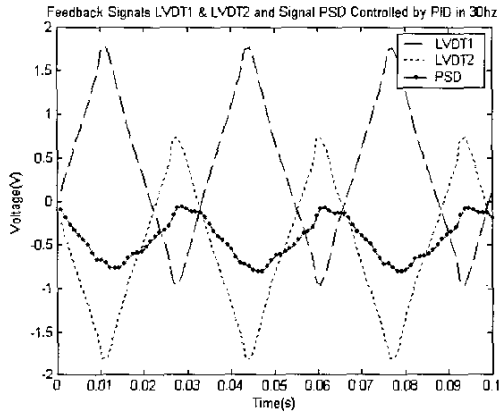

Fig. 16 The PID control, 128 resolution steps, 30 Hz repeat scanning.

The block diagram of the improved PID control is shown in Fig. 17. It likes a learning control way to improve the performance by the previous learning steps since our step-scan motion can be taken as two different repeat motions. One is the repeat stepping up and the other is the repeat stepping down. The following equations describe the improved PID controller :

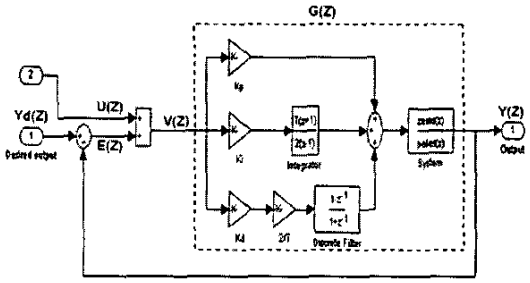

Fig. 17 Improved PID control block diagram.

$$u[k] = Q\left[u[k-1] + Le[k-1]\right] \tag{1}$$

$$e[k] = y_d[k] - y[k] \tag{2}$$

$$v[k] = u[k] + e[k] \tag{3}$$

The initial condition of u[0] is zero where Q and L are the designed factor. Eq. (4) is the recursive calculation of Eq. (1), we can get Eq. (4), and then add Eq. (4) into Eq. (3) which results in Eq. (5).

$$u[k] = L\left[Qe[k-1] + Q^2e[k-2] + \ldots + Q^ke[0]\right] \tag{4}$$

$$v[k] = e[k] + L\left[Qe[k-1] + Q^2e[k-2] + \ldots + Q^ke[0]\right] \tag{5}$$

Take Z transform of Eq. (5) results in Eq. (6). The open look equation from v[k] to y[k] can be illustrated in Eq. (7) and compare with simple PID controller which is illustrated in Eq. (8).

Take Z-transform of Eq. (5)

$$V(z) = E(z) + L\left[Qz^{-1}E(z) + Q^2z^{-2}E(z) + \ldots + Q^kz^{-k}E(z)\right]$$

$$= E(z)[1 + L(Qz^{-1} + Q^2z^{-2} + \ldots + Q^kz^{-k})]$$

$$= E(z)\left\langle 1 + \frac{LQz^{-1}[1-(Qz^{-1})^k]}{1-Qz^{-1}}\right\rangle$$

when $k \to \infty$

$$V(z) = E(z)(1 + \frac{LQz^{-1}}{1-Qz^{-1}}) \qquad \text{where} \left|Qz^{-1}\right| < 1 \tag{6}$$

$$Y(z) = G(z)V(z) = G(z)E(z)(1 + \frac{LQz^{-1}}{1-Qz^{-1}})$$

$$= G(z)[\frac{z+(L-1)Q}{z-Q}] \tag{7}$$

$$Y(z) = G(z)E(z) \tag{8}$$

For the simple PID system we can rewrite Eq. (8) to Eq. (9) and it is observable that the response time is defined at when G(z) is far greater then 1.

$$Y(z) = G(z)E(z) = G(z)[Y_d(z) - Y(z)]$$

$$\Rightarrow Y(z) = \frac{G(z)}{1+G(z)}Y_d(z)$$

$$\text{as } G(z) >> 1 \Rightarrow Y(z) = Y_d(z) \tag{9}$$

For the improved PID system we can rewrite Eq. (6) to Eq. (10) and it is obvious that the response time is defined at when G(z)[z+(L-1)Q] is far greater then (Z-Q). For more strictly limit the response time is reduced when G(z)(L-1)Q is far greater then –Q based on the simple PID controlled result in Eq.(9).

$$Y(z) = G(z)[\frac{z+(L-1)Q}{z-Q}]E(z)$$

$$= G(z)[\frac{z+(L-1)Q}{z-Q}][Y_d(z) - Y(z)]$$

$$\Rightarrow Y(z) = \frac{G(z)[z+(L-1)Q]}{(z-Q)+G(z)[z+(L-1)Q]}Y_d(z) \tag{10}$$

$$\text{as } G(z)[z+(L-1)Q] >> (z-Q) \text{ and } \left|Qz^{-1}\right| < 1$$

$$\Rightarrow Y(z) = Y_d(z)$$

The improved PID control has better performance than simple PID control from the proof of Eq. (9) and Eq. (10) since PID control will let G(z) >> 1 as times go on. The improved PID control based on the PID control results G(z) >> 1 and then we can assume zG(z) >> z. Thus the response time of the improved PID control is higher than PID control because that it pluses another demand G(z)(L-1)Q > Q which is designed to increase the convergence speed. The improved PID control results are illustrated in Fig. 18 and Fig. 19. Fig. 18 is the 1024 resolution step, 1 Hz repeat scanning result. The control results appears that that the feedback signals from LVDT sensors and the PSD sensors are almost the same. That means the settling response of each step within 1/1024 s is sufficient. Fig. 19 is the 128 resolution step, 30 Hz repeat scanning result. The control results appears that that the feedback signals from LVDT sensors and the PSD sensors are different and not accurate. That means the setting response of each step within 1/(128*30) s is not sufficient.

The experimental results from the PID control and the improved PID control are shown in Figs. 20~25, the control error from the improved PID is better than the simple PID control, which verifies the proof in the previous section. The comparison of the control error for 1 Hz and 1024 steps scan is shown in Figs. 20, 21. "Error1" represents the control error measured from the LVDT sensor "C". "Error2" represents the control error from the LVDT sensor "D". The comparison of the control error for 30 Hz and 128 steps scan shown in Figs. 22, 23. It is apparent that the control error response of 1 Hz 1024 resolution steps is better than 30 Hz 128 resolution steps, also confirming the earlier discussions. The improved PID control exhibits the learning control behavior. Thus, more leaning cycles resulted in better system performance. Figs. 24, 25 show the PSD detector signals, one also observes better control performance from the improved PID control.

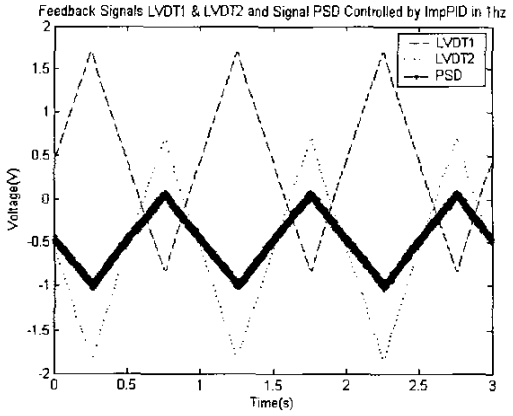

Fig. 18 Improved PID control, 1024 resolution steps, 1 Hz repeat scanning.

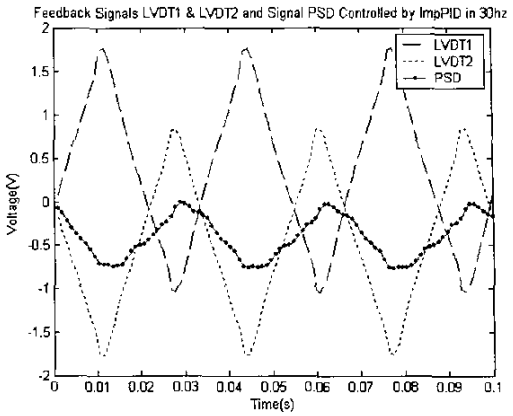

Fig. 19 Improved PID control, 128 resolution steps, 30 Hz repeat scanning.

V. CONCLUSIONS

This paper introduced a novel servo mechanism for an optical scanner design and used FEA software to analyze the structural mode shapes and the resonance frequencies. The knowledge about the resulted deformation also helps to form the basis of mechanism design. The simulation results are then compared with the experiments for validation. For the servo control design this paper proposed a modified PID controller. The modified PID control mimics the behavior of the learning control, but with much less memory requirement. The experimental results also show the superior performance from the proposed control.

ACKNOWLEDGEMENT

This research is supported by the Chung-Shan Institute of Science & Technology, contract No. NSC93-2623-7-002-006. Special thanks to Mr. Chin-Tei Lin in the Mechanism Research Design Lab. of National Taiwan University.

REFERENCES

[1] Y. Yeh, J. Yen, "A novel high-speed optical scanning platform", *Proceedings of SPIE* Vol.5638 Page352-361, Nov 2004

[2] Byoung Hun Kang, John T. Wen, Nicholas G. Dagalakis, Jason J. Gorman, "Analysis and design of parallel mechanisms with flexure joints" , *Processings of the 2004 IEEE Internatuinal Conference on Robotics & Automation*, pp299-311, New Orleans, LA, April 2004

[3] John E. Mclnroy, "Modeling and design of flexure jointed Stewart platforms for control purpose" *IEEE/ASME Transactions on mechatronics*, vol. 7, NO. 1, March 2002

[4] Lang Wu, *Electrical piezoelectricity and ceramics piezoelectricity*, pp.323-324, INFOWIDE BOOK COMPANY, Taiwan, Taipei, 1994

[5] Ansys release 8.0 help document, ANSYS

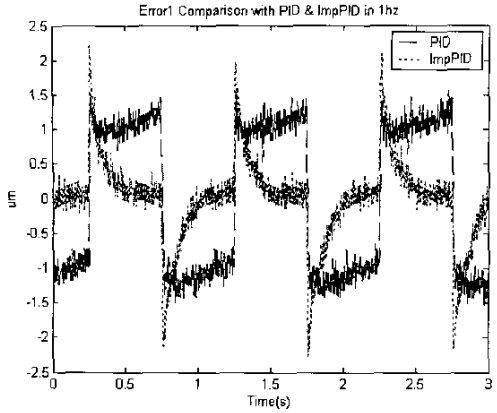

Fig. 20 1 Hz repeat scanning control error comparison of LVDT "C".

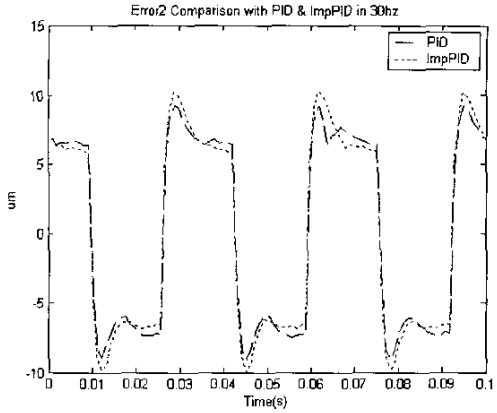

Fig. 23 30 Hz repeat scanning control error comparison of LVDT "D".

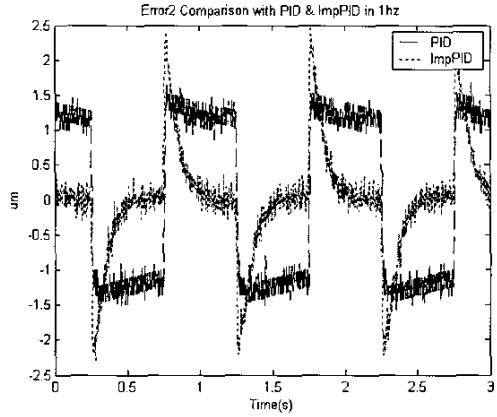

Fig. 21. 1 Hz repeat scanning control error comparison of LVDT "D".

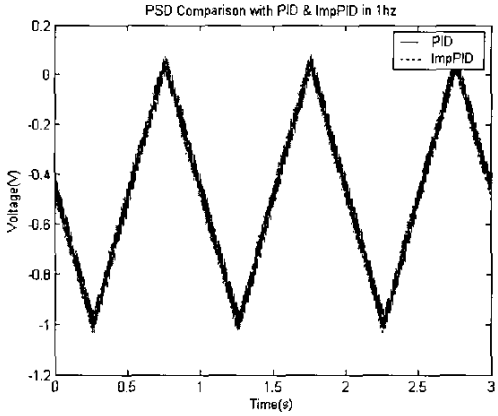

Fig. 24 1 Hz repeat scanning control PSD comparison.

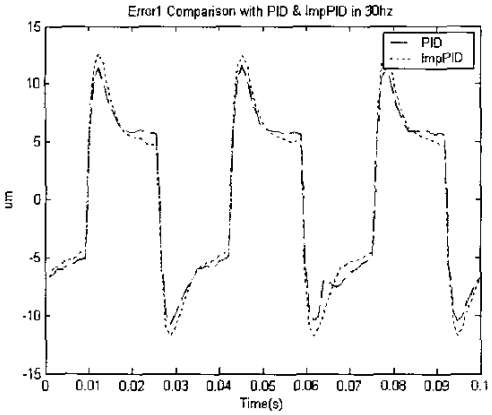

Fig. 22 30 Hz repeat scanning control error comparison of LVDT "C".

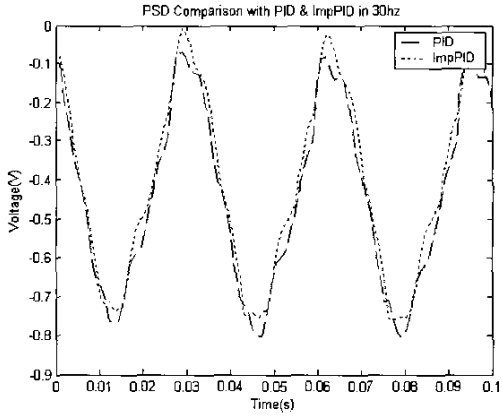

Fig. 25 30 Hz repeat scanning control PSD comparison.